International Journal of Geosciences, 2026, 17(9), 615-635
https://www.scirp.org/journal/ijg
ISSN Online: 2156-8367
ISSN Print: 2156-8359

Petro-Structural and Metallogenic Controls on Gold Mineralization at Sissingué, Syama-Boundiali Greenstone Belt, Northern Côte d'Ivoire

Ohouo Rebecca Mondah[1*], Kadio Aka Donald Koua[2], N'dri Eudes Sati Tegan[1], Marc Ephrem Allialy[1], Alain Nicaise Kouamelan[1]

[1]Laboratoire de Géologie, Ressources Minérales et Énergétiques (LGRME), UFR STRM, Université Félix Houphouët-Boigny Abidjan-Cocody, Abidjan, Côte d'Ivoire.
[2]Geology and Mineral Exploration Department, Zijin Mining Group Co., Ltd., Xiamen, China
Email: *rbecca.mondah@gmail.com, *mondah.rebecca74@ufhb.edu.ci

How to cite this paper: Mondah, O.R., Koua, K.A.D., Tegan, N.E.S., Allialy, M.E. and Kouamelan, A.N. (2026) Petro-Structural and Metallogenic Controls on Gold Mineralization at Sissingué, Syama-Boundiali Greenstone Belt, Northern Côte d'Ivoire. *International Journal of Geosciences*, **17**, 615-635.
https://doi.org/10.4236/ijg.2026.179029

Received: August 10, 2026
Accepted: September 8, 2026
Published: September 11, 2026

Abstract

Sissingué is located in northern Côte d'Ivoire within the Syama-Boundiali greenstone belt, a Paleoproterozoic segment of the West African Craton that hosts several structurally controlled gold systems. This paper reassesses the petro-structural and metallogenic controls on Sissingué mineralization using drill-core logging, petrographic and metallographic observations, collar and survey data, assay categories, selected numerical Au intervals, structural measurements, interpreted sections, and recent district-scale information. The drilled sequence is dominated by metaconglomerate, metasandstone, and metasiltstone intruded by granite, granodiorite, microgranite, and feldspar-porphyritic microgranite. Mineralization is preferentially associated with felsic intrusive rocks, intrusive contacts, and quartz-carbonate veins, although metasedimentary rocks are locally mineralized where they are altered and structurally prepared. The main ore-related assemblage is quartz-carbonate-sericite, with fine-grained pyrite and arsenopyrite as the principal sulfides. Structural data indicate a first-order NNE-SSW to NE-SW regional shear framework, overprinted by local NNW-SSE to N-S intrusive and vein trends. The highest-grade intervals are best explained by the intersection of favorable host rocks, reactivated structures, quartz-carbonate veining, and arsenopyrite-bearing alteration. Sissingué is therefore interpreted as a hydrothermal Birimian gold system controlled by both regional shear architecture and deposit-scale lithological and structural traps.

Keywords

Sissingué, Syama-Boundiali Belt, Birimian, Gold Mineralization, Petro-Structural Control

1. Introduction

The West African Craton hosts many of West Africa's major gold provinces. Its Paleoproterozoic Birimian domains are composed of volcano-sedimentary belts, metasedimentary basins, and granitoid domains affected by the Eburnean orogeny [1]-[5]. In these terranes, gold mineralization is commonly localized by long-lived shear zones, folds, faults, granitoid contacts, and hydrothermal alteration systems, although the relative roles of lithology, intrusion emplacement, and structural reactivation vary from one district to another [2] [4]-[6].

In Côte d'Ivoire, the Birimian formations cover a large part of the Precambrian basement and host numerous gold deposits and prospects. Recent studies of Ivorian gold districts, including Fettékro, Koffissiokaha, Kimoukro-Kokumbo, Marabadiassa-Katiola, and Souwa, show that gold is commonly associated with shear zones, lithological contacts, quartz or quartz-carbonate veins, sulfide-bearing alteration, and greenschist-facies assemblages [7]-[11]. These studies also show that detailed petrographic and structural work remains essential in areas where lateritic cover limits direct field observations.

The Sissingué gold system lies near Tengrela, close to the Mali border, within the Syama-Boundiali greenstone belt. The project was formerly described as the Tengrela or Sissingué Gold Project during feasibility-stage reporting [12]. Since production began, public reporting has treated Sissingué as a broader mining complex that includes the main pit and satellite deposits such as Fimbiasso and Bagoé [13]-[16]. This district-scale evolution is geologically important because it suggests that the Sissingué mineralization is part of a larger mineralized corridor rather than an isolated stock-hosted occurrence.

Previous work and current public descriptions indicate that the main Sissingué mineralization is structurally controlled and mainly hosted by a granitic to granodioritic stock and associated felsic dykes, with quartz-carbonate veining, pyrite, and arsenopyrite as key ore-related features [13] [14] [17]. However, the geometry of mineralization is not fully explained by the regional NNE-SSW to NE-SW Syama-Boundiali structural trend alone. At deposit scale, the mineralized intrusive bodies and many gold-bearing veins show an important NNW-SSE to N-S component. This contrast between regional shear architecture and local mineralized geometry is the central problem addressed in this paper.

The objective of this study is to refine the geological model of Sissingué using a petro-structural and metallogenic approach. The work combines drill-core information, petrographic observations, lithological and alteration data, selected Au intervals, and structural measurements to clarify how metasedimentary host rocks, felsic intrusions, hydrothermal alteration, and reactivated structures interact to localize gold. The paper focuses on geological controls that can guide further exploration and future analytical work.

2. Geological Context

2.1. Regional and Permit-Scale Framework

Sissingué is situated in northern Côte d'Ivoire, within the Syama-Boundiali greenstone belt (**Figure 1**). This belt links northern Côte d'Ivoire with southern Mali and forms part of the Paleoproterozoic metallogenic architecture of the southern West African Craton. At the regional scale, the lithological framework includes flysch-type metasedimentary rocks, intermediate volcanic rocks, local mafic intrusions, granitoids, and late sedimentary units [12]-[14]. The regional framework and location map used in **Figure 1** are based on the geological compilation of Graham [18].

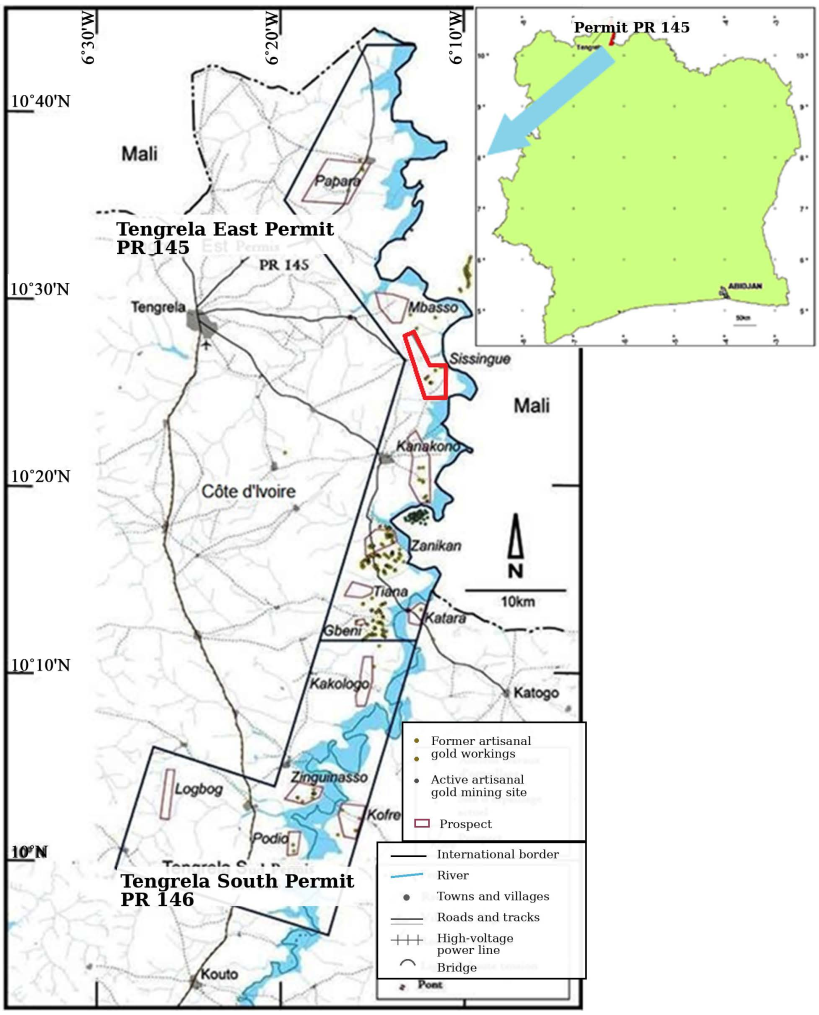

Figure 1. Location and regional framework of the Tengrela-Sissingué area, northern Côte d'Ivoire. The map places the Sissingué permit within the Côte d'Ivoire-Mali segment of the Syama-Boundiali corridor (after Graham [18], modified).

At permit scale, metasedimentary rocks and felsic intrusive bodies are cut by major NNE-SSW to NE-SW structures (**Figure 2**). The permit-scale geology and interpreted local lineaments used in **Figure 2** are based on the Occidental Gold SARL Tengrela report [19]. This framework is consistent with Birimian gold systems in which regional deformation provides the first-order permeability architecture, while local lithological contrasts and reactivated structures control deposit-scale mineralization [6] [11].

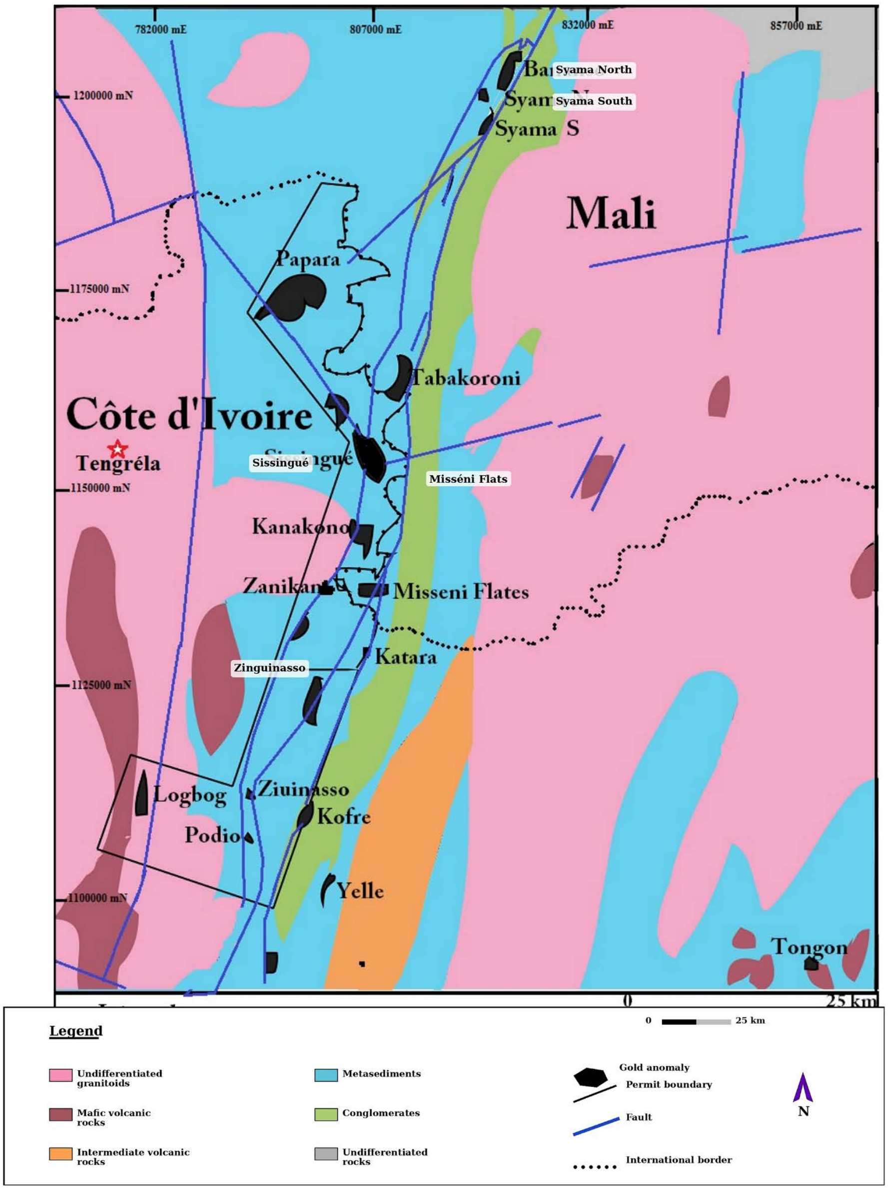

Figure 2. Permit-scale geology and interpreted structural framework of the Sissingué area. The map shows the Syama-Boundiali structural corridor, local lineaments, metasedimentary units and granitoid/intrusive domains (after Occidental Gold SARL [19], modified).

2.2. Sissingué District Context from 2014 to 2026

Since 2014, the geological context of Sissingué has shifted from a single-deposit feasibility model to a district-scale mining complex. Current public information describes high-grade ore from the main pit and satellite open pits processed through a conventional 1.4 Mt/a CIL plant [13]. Development of the Fimbiasso and Bagoé satellite deposits has extended the mine life to 2030 [13]. The main public updates relevant to the geological interpretation are summarized in **Table 1**.

Table 1. Public 2014-2026 updates relevant to the geological interpretation of Sissingué.

Period	Update	Geological relevance
2014-2015	NI 43-101 and feasibility reporting established the baseline geological and project framework.	Starting point for deposit-scale interpretation.
2018	Sissingué entered production as Perseus's second gold mine.	Allows the geology to be discussed in an operating-mine context.
2021-2026	Public descriptions emphasize a main pit plus satellite deposits within trucking distance of the plant.	Supports a district-scale model rather than an isolated pit model.
2025	Public resources and reserves include Fimbiasso and Bagoé in addition to Sissingué.	Confirms that current reporting treats Sissingué as a complex.
2026	Bagoé ore was introduced after Fimbiasso mining, improving the complex through higher-grade feed.	Highlights the value of structurally controlled satellite deposits.

This update has geological significance. Public mineral resource and ore reserve information now includes Fimbiasso and Bagoé in addition to the Sissingué Gold Mine [15]. In the December 2025 quarter, ore from Bagoé was introduced after Fimbiasso mining, showing the importance of satellite mineralization in the same district [16]. These updates support a corridor-scale model rather than a narrow main-pit model.

2.3. Deposit-Scale Geology

At deposit scale, public descriptions and drill-core observations converge on a similar model. Gold occurs mainly within a plug-like granodiorite or granitic intrusion and a felsic dyke system intruded into argillite, siltstone, sandstone, heterolithic sedimentary breccia, and conglomerate along an approximately 700 m long and 250 m thick NNW-trending corridor [14]. Mineralization is concentrated in intrusive rocks and dykes, but metasedimentary rocks above and around the intrusion can also be strongly mineralized [14].

The principal hydrothermal assemblage is quartz-carbonate veining with carbonate, sericite, albite, pyrite, and arsenopyrite alteration [13] [14]. At the main pit, gold-bearing veins commonly trend NNW to N-S and dip steeply, while disseminated mineralization occurs in alteration envelopes around mineralized quartz veins [13]. These relationships place Sissingué within the family of structurally controlled, greenstone-hosted hydrothermal gold systems, with a strong local intrusive and contact control.

3. Materials and Methods

3.1. Data Compilation and Validation

The main datasets used in this study are summarized in **Table 2**. The study uses collar, downhole survey, geology, assay-category, selected numerical Au, geotechnical, and structural datasets supplied for Sissingué. The internally consistent drill-core subset used for detailed integration is SD275-SD282. Selected numerical Au intervals from SD112, SD154, SLC230, and SLC232 were used only for section-scale grade-lithology comparison. The Au_cat field was treated as a categorical mineralization class and not as a continuous gold-grade variable.

Table 2. Main datasets used in this study.

Dataset	Content	Use
Collar	SD275-SD282 collar coordinates, depth, dip and azimuth	Drill-hole location and starting geometry
Survey	91 downhole survey records	Drill-hole deviation and structural orientation support
Geology	2231 interval-based geological logs	Lithology, alteration, sulfides and veins
Assay category	2082 Au_cat intervals	Mineralization classification only
Selected sections	Numerical Au intervals from selected sections	Section-scale grade-lithology comparison
Structural data	Computed structural-orientation records	Vein, fault/fracture, broken-zone, joint and contact analysis

The selected numerical Au dataset comprises all available intervals from the section files for SD112 (0 - 157 m), SD154 (73 - 168 m), SLC230 (0 - 140 m), and SLC232 (32 - 120 m). Low-grade and apparently unmineralized intervals were not removed; the dataset includes background values as low as 0.01 g/t Au and high values up to 85.00 g/t Au. Because these intervals were selected from section data rather than extracted from a full validated continuous assay database, they are used only to test grade-lithology relationships at section scale.

Data validation focused on hole identifiers, interval continuity, depth compatibility, and lithology-assay matching. Where geology, assay-category, and structural intervals did not have identical boundaries, matches were made by interval overlap. The overlap length was calculated as min (TO1, TO2) - max(FROM1, FROM2); only positive overlaps were retained. For one-to-many matches, the overlapping interval was split into its component overlap segments, and lithology, Au_cat, alteration, sulfide, and structure attributes were assigned to each segment. Length-weighted summaries were used for lithology-mineralization comparisons, whereas raw record counts were used only for inventory descriptions. Intervals lacking lithological or depth information were excluded from quantitative comparisons but retained, where appropriate, for qualitative geological interpretation.

The Au_cat class definitions used for categorical comparison are provided in

Table 3. The Au_cat classes were used as ordered mineralization classes supplied with the assay-category table, not as measured continuous Au grades. Classes A-C were treated as the "higher Au_cat" group in Figure 9 because they correspond to intervals with category labels of 1.2 g/t Au or greater. Comparisons with lithology were made by overlap length so that longer intervals did not receive the same weight as shorter intervals merely because they formed one record.

Table 3. Definition of Au_cat classes used for categorical mineralization comparison.

Class	Category label in supplied data	Interpreted Au range or meaning	Use in this paper
A	5	≥ 5 g/t Au category	Higher Au_cat
B	3.0 - 5	3.0 - 5.0 g/t Au category	Higher Au_cat
C	1.2 - 3	1.2 - 3.0 g/t Au category	Higher Au_cat
D	0.8 - 1.2	0.8 - 1.2 g/t Au category	Intermediate
E	0.2 - 0.5	0.2 - 0.5 g/t Au category	Low
F	0.1 - 0.2	0.1 - 0.2 g/t Au category	Low
G	0.1	≤0.1 g/t Au/background category as supplied	Background/very low

3.2. Petrographic and Mineralogical Observations

Because outcrops are scarce and the area is largely covered by laterite, petrographic interpretation relied mainly on drill-core observations, hand specimens, and thin sections. Core and hand specimens were described using texture, structure, color, degree of alteration, sulfide content, and mineral assemblage. Selected samples were prepared as polished or uncovered thin sections for microscopic observation at the Basement Geology and Metallogeny Laboratory. These observations were used to refine field names, identify alteration minerals, and distinguish metasedimentary host rocks from intrusive phases.

Chemical analyses for gold were undertaken by fire assay in Ghana. Blank, certified reference material, and duplicate samples were inserted in the original exploration batches. However, the dataset supplied for the present academic reassessment does not include the original laboratory certificates, batch-level detection-limit sheets, insertion-rate table, or documented failed quality-control batches. For this reason, numerical Au data are used only where they are tied to selected section intervals, and the Au_cat table is treated strictly as a categorical mineralization dataset. If a blank, standard, or duplicate had failed the project acceptance criteria in the original QA/QC workflow, the affected batch would have required quarantine, laboratory investigation, and re-assay before being accepted into the validated database; no such failed batch information was available in the files used here.

3.3. Structural Measurements and Orientation Treatment

Structural observations focused on veins, faults, fractures, joints, broken zones, lithological contacts, and mineralized structures in oriented drill core. Alpha-beta measurements were obtained using a kenometer/goniometer and converted using drill-hole orientation information (Figure 3). Rose diagrams and selected sections were then used to compare regional NNE-SSW to NE-SW structures with deposit-scale NNW-SSE to N-S mineralized trends.

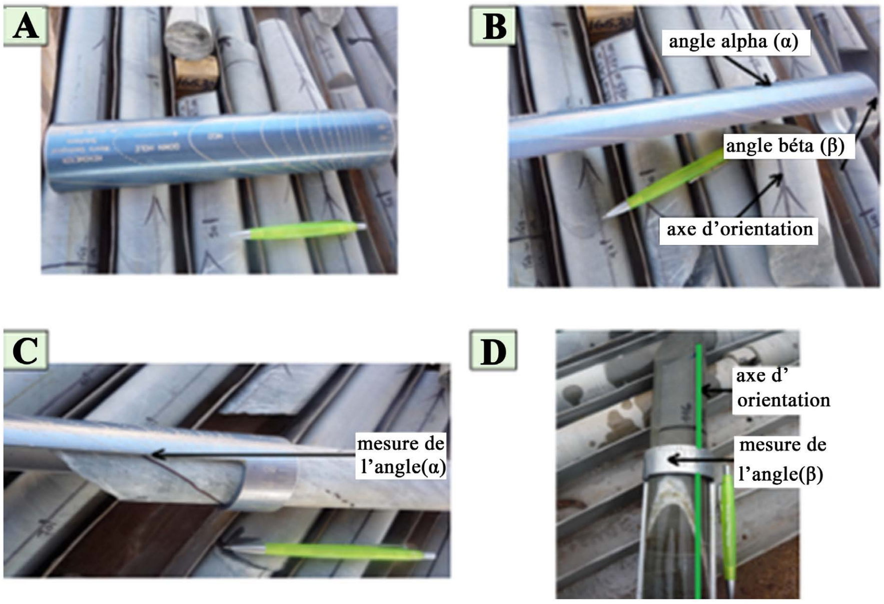

Figure 3. Method used to measure structural elements on oriented drill core with a kenometer. (A) Kenometer model; (B) alpha and beta angles relative to the core orientation line; (C) measurement of the alpha angle; (D) measurement of the beta angle. These measurements were corrected using drill-hole survey data before structural interpretation.

3.4. Modelling and Conceptual Integration

Collar and survey data, lithological logs, structural records, Au_cat classes, and selected numerical Au intervals were integrated to build a consistent geological interpretation. The modelling workflow shown in Figure 4 is conceptual and supports geological interpretation; it is not a resource model. Its purpose is to show how validated drilling data can be transformed into lithological, structural, and mineralized envelopes for future work in Leapfrog Geo, Micromine, or equivalent software.

4. Results

4.1. Petrography of Host Rocks and Intrusive Units

The drilled sequence is composed of metasedimentary rocks intruded by felsic to intermediate magmatic rocks. The principal metasedimentary rocks are metaconglomerate, metasandstone, metasiltstone, and graphitic schist (Figure 5). Metaconglomerate is polymictic and contains rounded to subrounded clasts of quartz, metasiltstone, and unidentified lithic fragments in a silicified greywacke matrix. Metasandstone is grey-green to dark grey and locally sulfide-bearing near intrusive contacts and veins. Metasiltstone and graphitic schist are darker, locally foliated, and may contain coarse pyrite and graphite, but they are less consistently associated with high Au or arsenopyrite than the intrusive units.

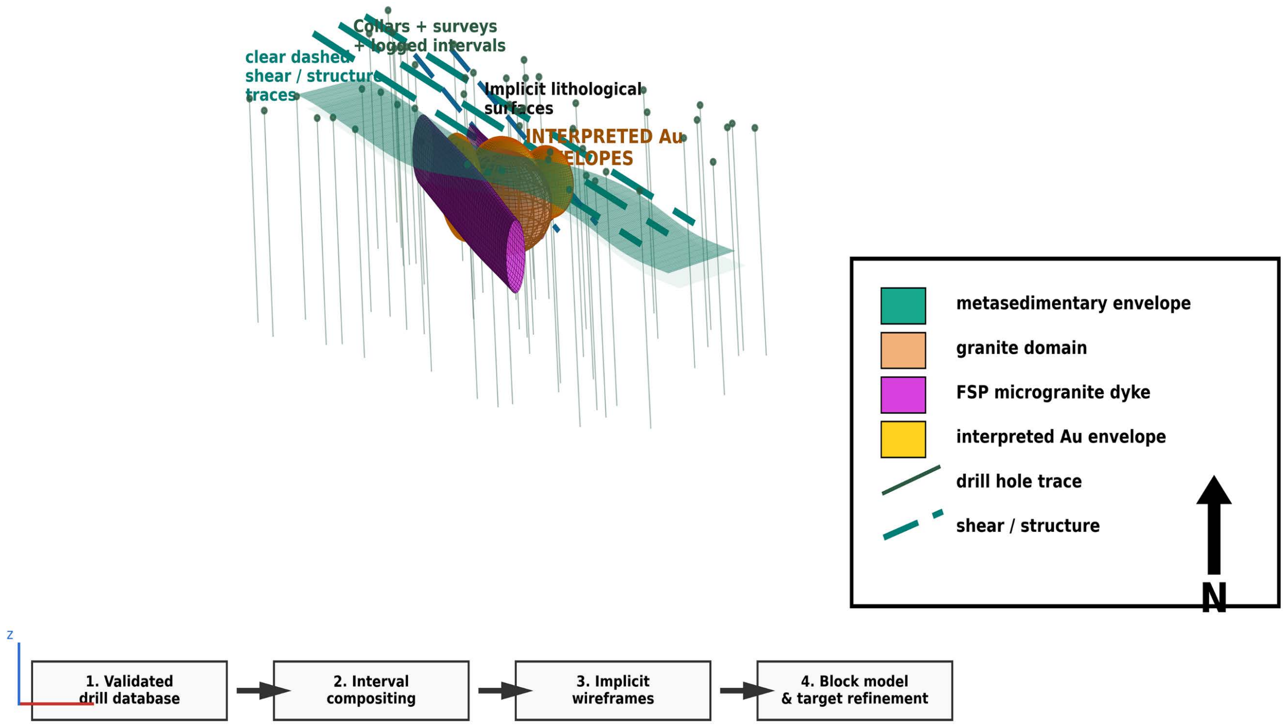

Figure 4. Conceptual workflow for implicit 3D geological modelling of the Sissingué gold system. Collar and survey data, lithological logs, assay information, structural measurements, and interpreted sections are integrated to build lithological, structural, and mineralized domains. The output is a geological framework for target refinement and future resource work, not a resource estimate.

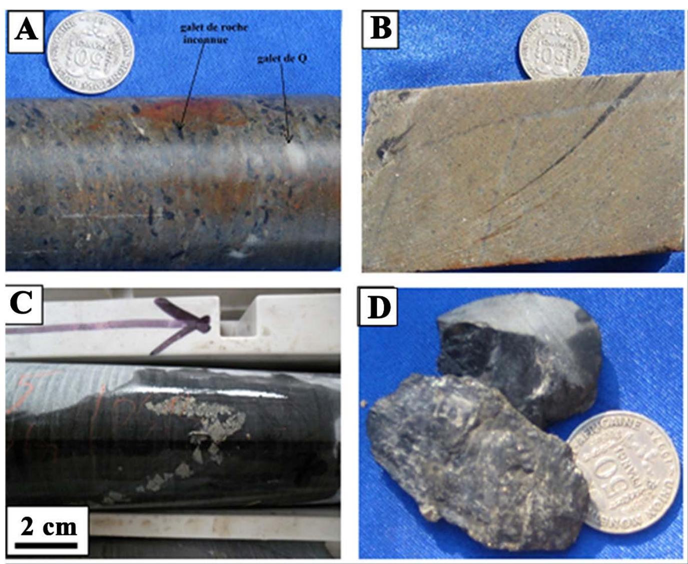

Figure 5. Macroscopic aspects of metasedimentary rocks observed at Sissingué. (A) Metaconglomerate showing lithic clasts and quartz pebbles; (B) metasandstone; (C) metasiltstone with quartz and sulfide-bearing bands; (D) graphitic schist showing fissility and graphite on fracture surfaces.

The intrusive units include microgranite, feldspar-porphyritic microgranite, porphyritic microgranodiorite, and minor volcanic or volcaniclastic rocks. Feldspar-porphyritic microgranite is leucocratic, massive, and commonly contains feldspar phenocrysts. It is relatively rich in fine sulfides, especially disseminated arsenopyrite and sulfides along quartz-vein margins (Figure 6(A), Figure 6(B)). Microscopically, it contains quartz, orthoclase, and plagioclase phenocrysts, calcite, sericite, and opaque minerals.

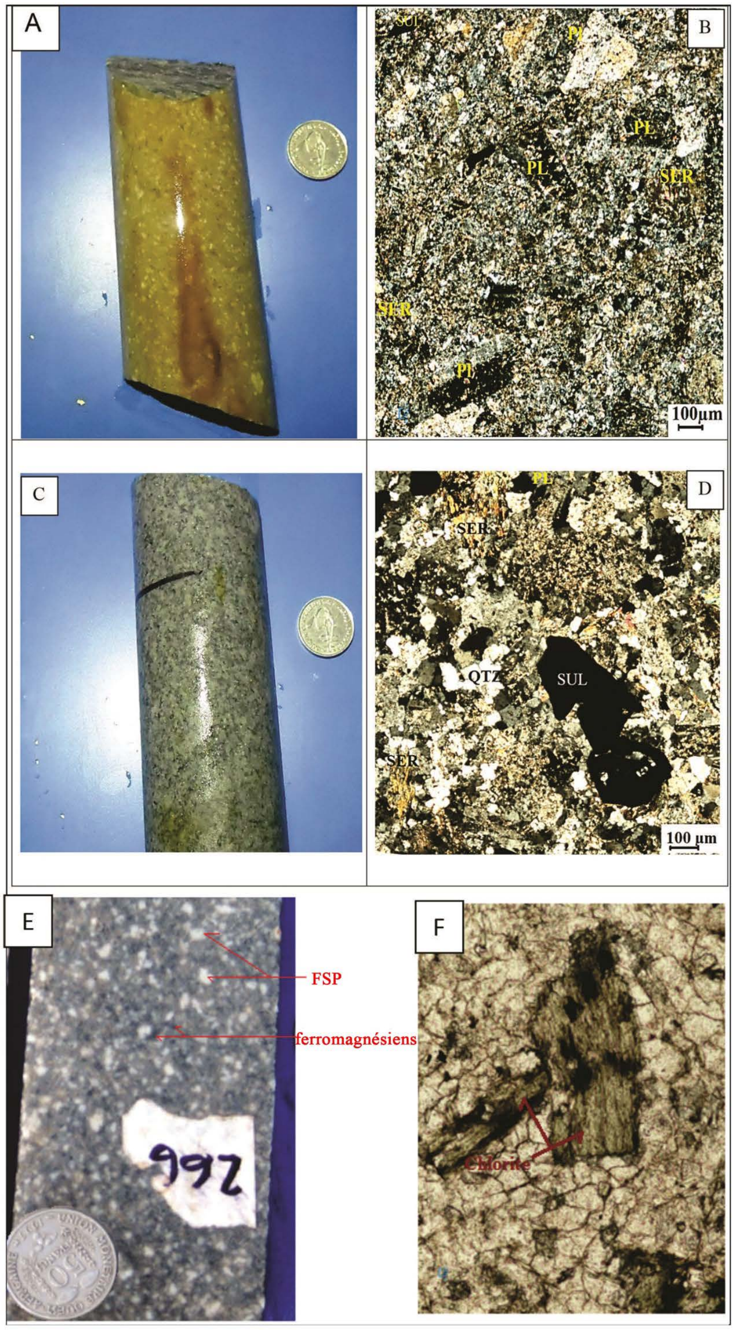

Figure 6. Macroscopic and microscopic features of intrusive units. (A-B) Feldspar-porphyritic microgranite; (C-D) microgranite; and (E-F) porphyritic microgranodiorite.

Microgranite is leucocratic and fine-grained, with rare quartz phenocrysts in a matrix where minerals are difficult to identify macroscopically. In thin section, it contains corroded quartz, plagioclase, lamellar muscovite, fibrous sericite aggregates, carbonates, and opaque minerals (Figure 6(C), Figure 6(D)).

Porphyritic microgranodiorite is darker, commonly chlorite-rich, and appears less mineralized than the sericite-bearing feldspar-porphyritic microgranite (Figure 6(E), Figure 6(F)).

The plates show feldspar phenocrysts, quartz veinlets, arsenopyrite/sulfide occurrences, sericite-bearing feldspar-porphyritic microgranite, and chlorite-rich microgranodiorite. These features distinguish the more mineralized sericite-bearing felsic dyke facies from the darker chlorite-rich microgranodioritic facies.

4.2. Lithological Architecture and Downhole Distribution

The SD275-SD282 drill logs show that metasedimentary rocks dominate the drilled sequence. Metaconglomerate is the most abundant unit, followed by metasiltstone and metasandstone (Table 4; Figure 7). Intrusive rocks form a smaller proportion of the logged meters, but they are disproportionately important for mineralization because high Au_cat intervals and selected numerical Au values are commonly associated with granite and feldspar-porphyritic microgranite.

The interpreted architecture consists of a metasedimentary package intruded by a compact granitic body and feldspar-porphyritic microgranite dykes (Figure 8). The dykes and mineralized zones show a strong NNW-SSE component, oblique to the broader NNE-SSW to NE-SW regional structural grain. Mineralized envelopes are therefore interpreted around the intrusive body, dyke margins, and adjacent altered metasedimentary rocks rather than within a single homogeneous host.

The simplified downhole lithology confirms that higher Au_cat intervals are not randomly distributed through the section (Figure 9). They commonly occur within or near intrusive rocks and along intervals where lithological contacts and vein-bearing zones are present. Because Au_cat is categorical, the figure is used to compare mineralization classes with lithology, not to calculate grade statistics.

Table 4. Logged lithological distribution in SD275-SD282.

Lithological unit	Logged meters	Percent	Interpretation
Metaconglomerate	1089.0	46.8	Dominant metasedimentary host rock
Metasiltstone	409.9	17.6	Fine-grained metasedimentary unit
Metasandstone	377.5	16.2	Common metasedimentary host rock
Feldspar-porphyritic microgranite	188.8	8.1	Dyke-like intrusive host

Continued

Granite	122.6	5.3	Favorable intrusive host
Laterite	105.3	4.5	Weathered cover
Undifferentiated	18.0	0.8	Minor logged category
Clay-rich cover	14.0	0.6	Weathered cover
Granodiorite	2.2	0.1	Minor intrusive phase

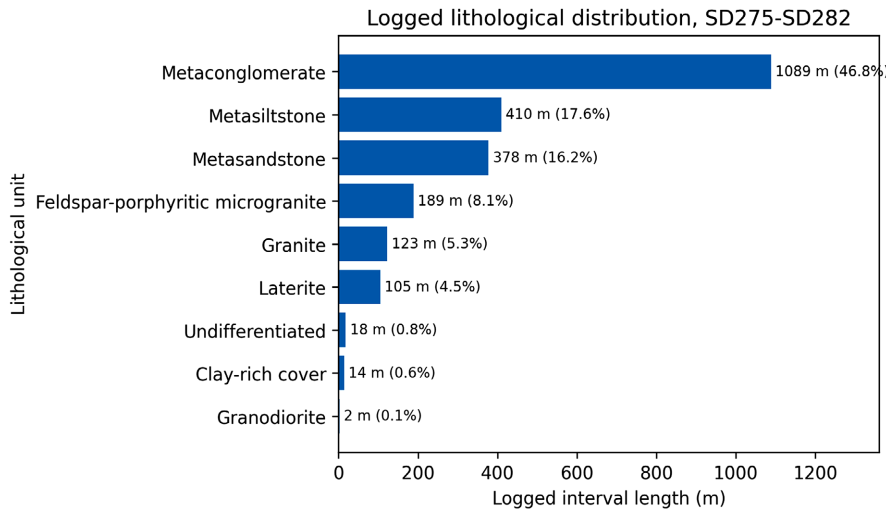

Figure 7. Logged lithological distribution in the SD275-SD282 drill-hole dataset. Metasedimentary rocks dominate the logged metres, whereas granite and feldspar-porphyritic microgranite represent smaller but metallogenically important units.

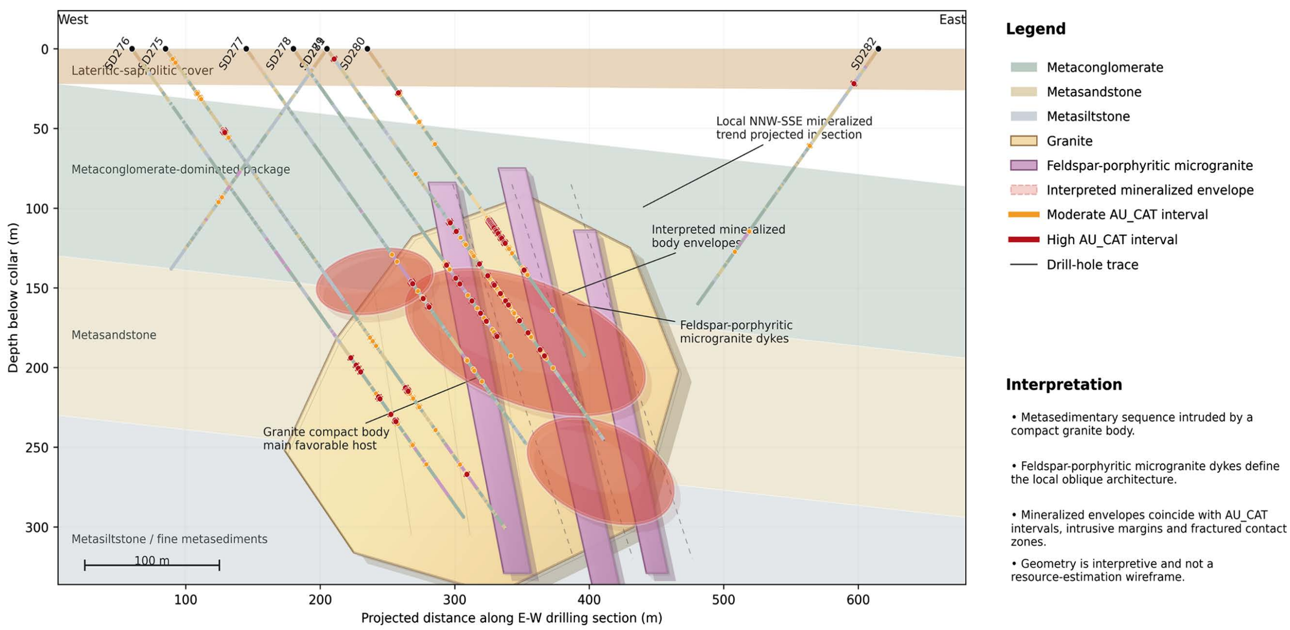

Figure 8. Lithological architecture and interpreted mineralized-body geometry. The model illustrates the relationship between metasedimentary rocks, granite, feldspar-porphyritic microgranite, and interpreted mineralized envelopes. It is a geological interpretation based on section-scale relationships and is not a resource-estimation wireframe.

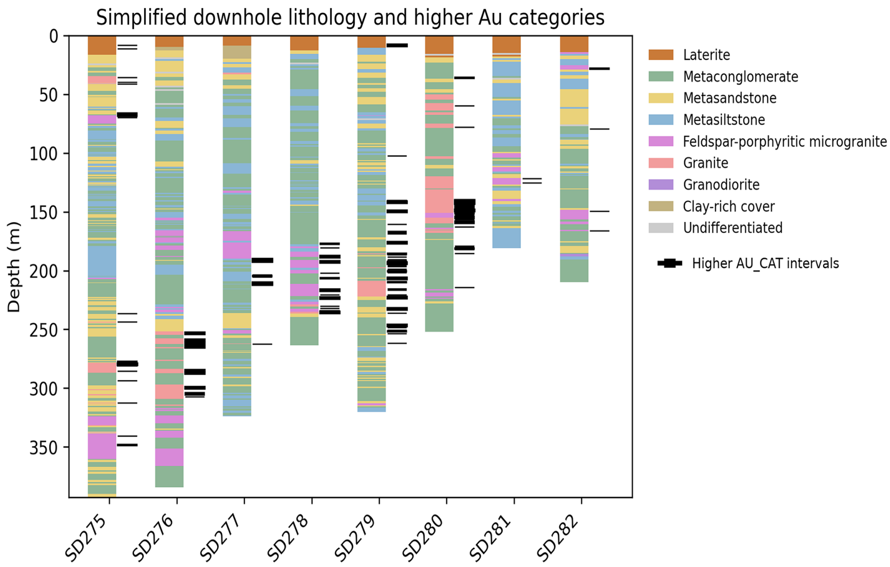

Figure 9. Simplified downhole lithology and higher Au_cat intervals for SD275-SD282. Au_cat values are categorical and are used only as mineralization classes. The black markers highlight intervals assigned to higher Au_cat classes and show their spatial relationship with intrusive rocks, contacts, and altered metasedimentary units.

4.3. Alteration, Sulfides and Mineralization Style

Hydrothermal alteration is dominated by quartz-carbonate-sericite assemblages. The strongest mineralized intervals are generally those where felsic intrusive rocks or nearby metasedimentary rocks are cut by quartz-carbonate veins and contain sulfides. Pyrite is widespread and therefore not diagnostic on its own. Arsenopyrite is more useful as an ore indicator because it is repeatedly associated with mineralized intervals and quartz-carbonate-sericite alteration.

Representative core photographs, hand specimens, and photomicrographs show the main mineralization features (Figure 10). Native gold and pyrrhotite were observed in some samples, and arsenopyrite occurs along veins and in altered intrusive rocks. These relationships support two linked mineralization styles: disseminated sulfide-bearing mineralization in felsic intrusions and locally in metasediments, and vein-hosted mineralization in quartz and quartz-carbonate veins. These styles are not separate deposit types; they are parts of the same hydrothermal system developed where fluids used fractures, vein networks, and intrusive contacts as pathways.

4.4. Selected Au Values and Lithological Association

Selected numerical Au values indicate that granite contains the highest observed values in the available section-scale dataset (Figure 11). Feldspar-porphyritic microgranite is also mineralized, and metasedimentary units contain local mineralized intervals where they are altered or cut by veins. Because these are selected intervals, they are used to test geological relationships and not to calculate a deposit-wide grade distribution.

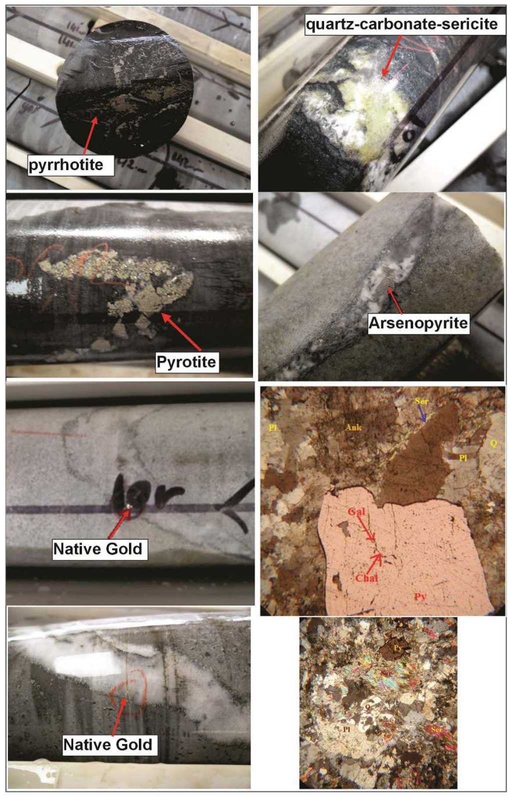

Figure 10. Representative lithological, alteration, and mineralization evidence from drill core, hand specimens, and microscopy. The plates show fresh and altered intrusive rocks, visible gold occurrences, arsenopyrite-bearing zones, quartz-carbonate veins, and sulfide-bearing altered rocks that support the interpretation of disseminated and vein-hosted mineralization.

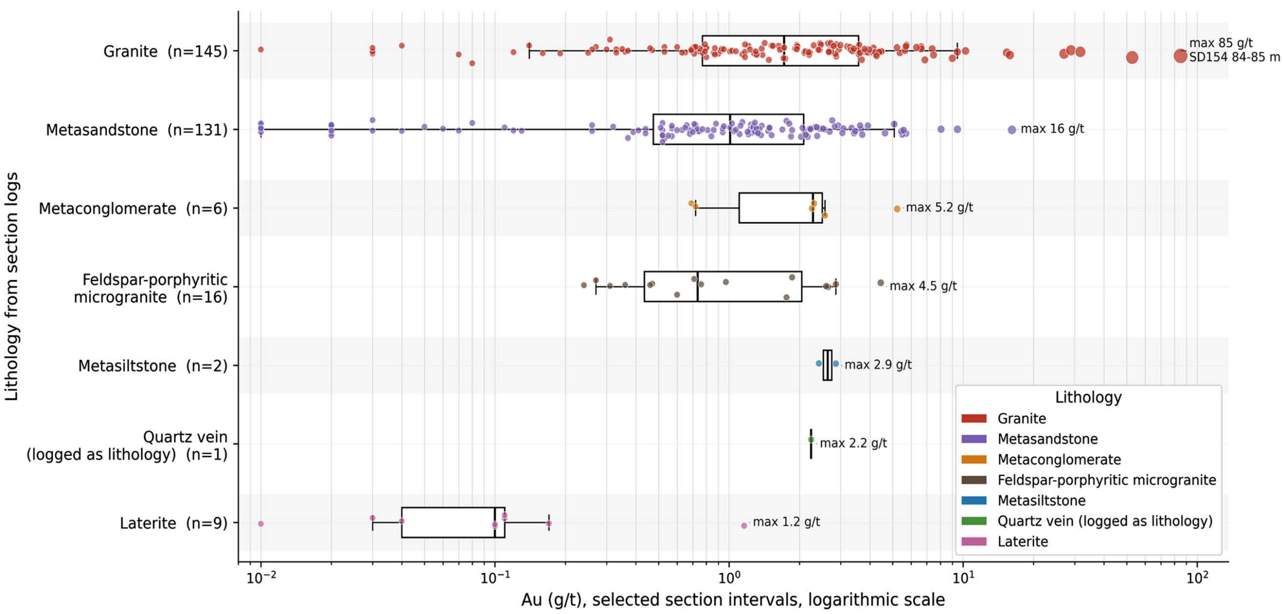

Figure 11. Selected numerical Au values by lithology from section intervals. Values are plotted on a logarithmic scale and used only for section-scale comparison. They show that high Au values are preferentially associated with granite and, to a lesser degree, feldspar-porphyritic microgranite and altered metasedimentary units.

4.5. Structural Controls

The structural dataset used for Figure 12 contains 1,453 non-duplicate orientation records after cleaning. Veins are the most abundant structures, followed by faults/fractures, broken zones, joints, and contacts. The grouped vein rose diagram in Figure 12 uses 690 filtered vein records with complete structure type and orientation information. This filtered denominator differs from the raw per-hole vein counts shown in Figure 13 because the latter are source-figure labels from selected drill holes and include records not used in the cleaned grouped rose diagram.

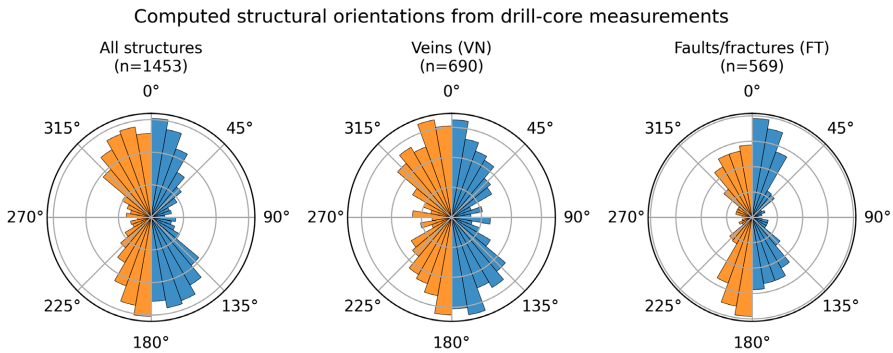

Figure 12. Rose diagrams of computed structural orientations from drill-core measurements. The diagrams summarize the cleaned structural dataset: all structures (n = 1453), veins retained for the grouped rose diagram (n = 690), and faults/fractures (n = 569). Counts refer to filtered orientation records with usable structure type and orientation information.

Core-scale observations support structural interpretation. Quartz veins, fractures, and faults are distinguished from fractures by the presence of tectoglyphs such as slickensides or striations indicating the direction of slip, contacts, and broken zones are common in the mineralized intervals (Figure 13). Several veins are fractured, sheared, or brecciated, indicating repeated opening and reactivation. These features are consistent with hydrothermal fluid flow through structurally prepared rocks.

5. Discussion

5.1. A District-Scale System, Not Only a Main-Pit Model

The 2014-2026 information changes the way Sissingué should be discussed. The original feasibility-stage deposit remains the geological reference point, but the current Sissingué Complex includes satellite sources such as Fimbiasso and Bagoé [13] [15] [16]. This broader context matters because it shows that similar structural and alteration controls recur at district scale.

The exploration-pipeline description is particularly useful. It places Sissingué in clastic basinal metasediments intruded by felsic and granodioritic bodies, cut by NNE-trending shears and faults, with mineralization concentrated in a plug-like granodiorite and felsic dyke system along a NNW-trending corridor [14].

Fimbiasso and Bagoé further support the idea that mineralization in the district is controlled by rheological contrast, deformation zones, quartz-carbonate veining, sericite-carbonate alteration, pyrite, and arsenopyrite [14].

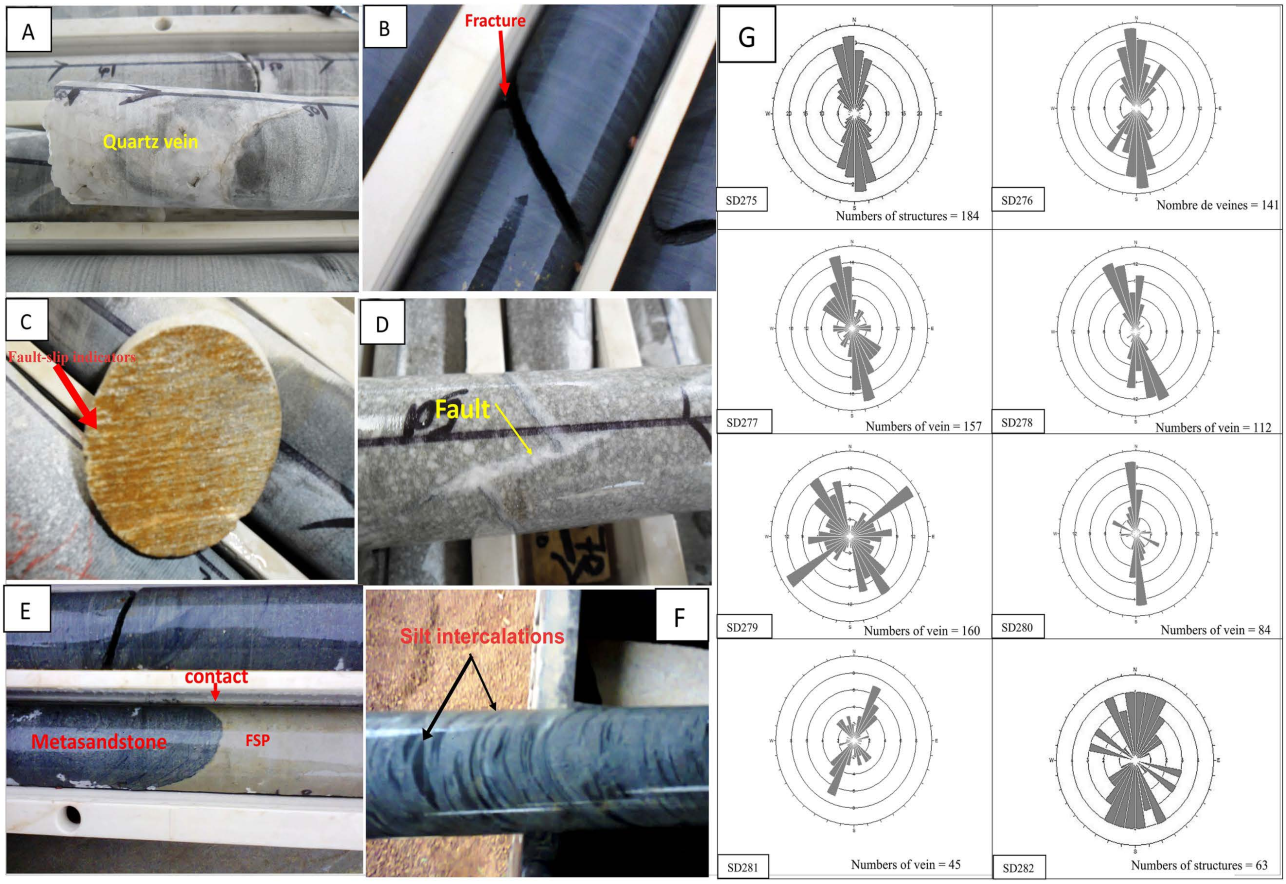

Figure 13. Core-scale structural evidence and vein orientations. The figure shows (A) quartz veins, (B) natural fractures, (C) slickensides or striations indicating fault-slip direction, (D) quartz-filled faults, (E) contacts between metasandstone and feldspar-porphyritic microgranite, (F) silt intercalations within metasandstones, and (G) rose diagrams of vein orientations in selected drill holes. The counts displayed inside the individual rose diagrams are raw selected-hole labels; the cleaned grouped vein denominator used in Figure 12 is n = 690.

5.2. Lithological Control: Host and Trap Rather than Source

The association between gold and felsic intrusive rocks is clear, but it should be interpreted carefully. Microgranite, microgranodiorite, and feldspar-porphyritic microgranite are favorable hosts because they are competent, fractured during deformation, and provide contacts that focus fluid flow. The available data do not prove that these intrusions were the metal source. They are better described as mechanical and lithological traps within a broader shear-hosted hydrothermal system.

Metasedimentary rocks remain significant. Public descriptions indicate that metasediments above the main feldspar-porphyritic microgranite body can be strongly mineralized [14], and the section data show locally mineralized metasandstone and metaconglomerate. A target model restricted to microgranite would therefore be incomplete. The best exploration sites are likely to occur where felsic intrusive rocks, sedimentary contacts, vein density, and arsenopyrite-bearing alteration coincide.

5.3. Hydrothermal and Sulfide Controls

The most consistent ore-related assemblage at Sissingué is quartz-carbonate-sericite with pyrite, arsenopyrite, and pyrrhotite. This assemblage is broadly compatible with nearby Boundiali-Syama studies, where sericite-, carbonate-, and sulfide-rich alteration is repeatedly linked to gold enrichment [20] [21]. The comparison reinforces a practical point: pyrite alone is not sufficient as an ore vector, whereas arsenopyrite in sericite-carbonate altered zones is a stronger indicator of mineralization.

The selected section data and public geological descriptions both show that mineralization can be disseminated or vein-hosted. These styles are linked by the same fluid-flow system. Quartz-carbonate veins created pathways and depositional sites; alteration envelopes around these veins allowed sulfide precipitation; and arsenopyrite-bearing zones mark the most favorable parts of the system. The model is therefore hydrothermal and structural but strongly filtered by lithology.

5.4. Structural Control and Local Reactivation

The main structural issue at Sissingué is the contrast between regional and local trends. Regionally, the Syama-Boundiali belt is organized by NNE-SSW to NE-SW shear zones. Locally, the mineralized intrusive corridor and many gold-bearing veins show NNW-SSE to N-S orientations. This obliquity is not a contradiction; it is the feature that explains mineralization localization.

A plausible interpretation is that the regional shear corridor supplied the first-order permeability architecture, while local oblique structures, dyke margins, and contacts created deposit-scale traps. This is consistent with the Syama deposit, where regional structures, brittle-ductile deformation, and hydrothermal alteration acted together to focus gold [22], and with broader Birimian orogenic gold models that emphasize repeated deformation and fluid flow along faults, shears, and competent lithological contacts [6] [23] [24].

5.5. Conceptual Petro-Structural Model

The model proposed here links four elements (**Figure 14** and **Figure 15**). First, Birimian metasediments formed the main host sequence. Second, microgranite, granodiorite, and feldspar-porphyritic microgranite intruded the sequence and introduced rheological contrasts. Third, regional shear deformation and later reactivation produced faults, fractures, and quartz-carbonate vein networks. Fourth, hydrothermal fluids deposited pyrite, arsenopyrite, and gold where veins, contacts, and altered intrusive or sedimentary rocks provided open pathways and reactive sites.

This is a petro-structural and metallogenic model, not a complete genetic model. The available data do not constrain the age of the intrusive phases, the timing of mineralization, the gold source, or the fluid chemistry. These questions require U-Pb dating of intrusive rocks, dating of hydrothermal minerals where possible, whole-rock geochemistry, sulfide trace-element work, fluid inclusions, and stable isotopes.

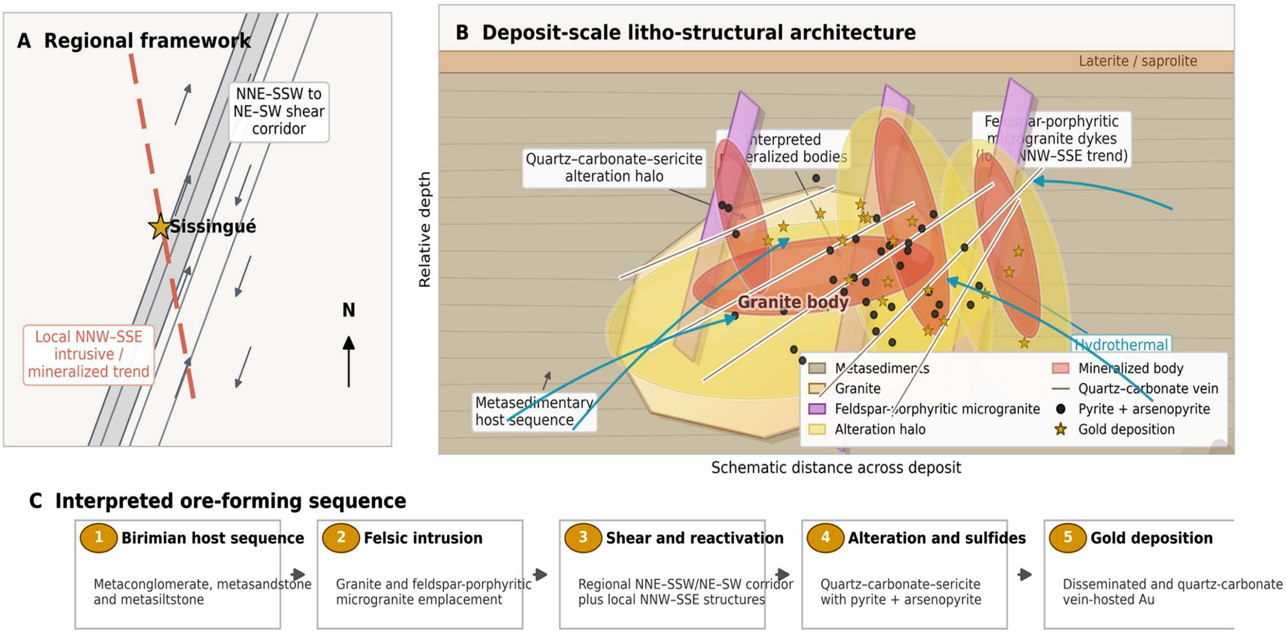

Figure 14. Conceptual petro-structural model for gold mineralization at Sissingué. The model links the regional Syama-Boundiali shear corridor with local intrusive and structural trends, quartz-carbonate-sericite alteration, pyrite-arsenopyrite development, and gold deposition. It represents an interpreted petro-structural control rather than a fully constrained genetic model.

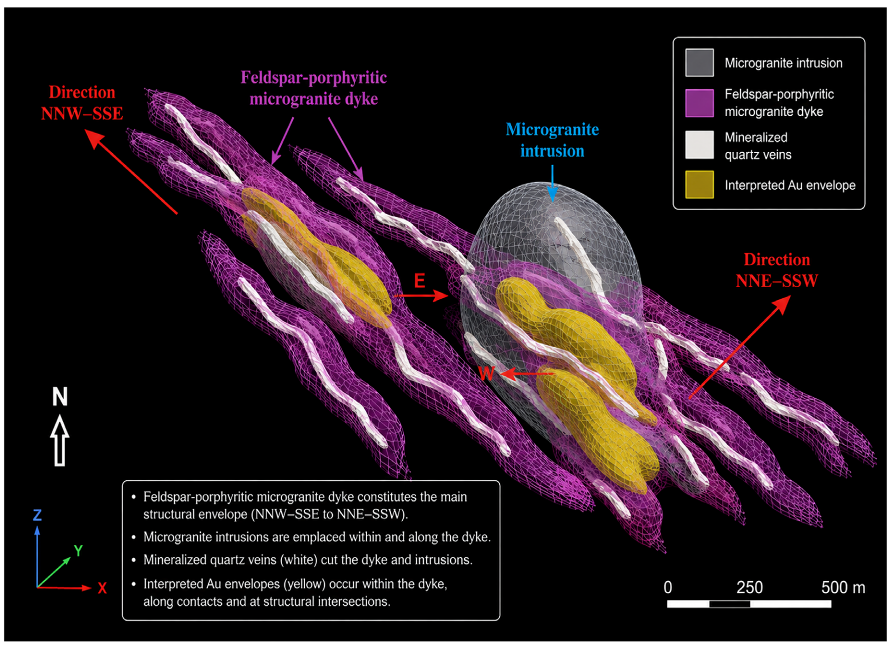

Figure 15. 3D geological model of the Sissingué mineralized system. Feldspar-porphyritic microgranite dykes define the main NNW-SSE to NNE-SSW intrusive-structural corridor and host microgranite intrusions, mineralized quartz veins, and interpreted Au envelopes.

6. Conclusions

Sissingué is best interpreted as a structurally controlled Birimian hydrothermal gold system developed within the Syama-Boundiali greenstone belt. The mineralized system is hosted by metasedimentary rocks intruded by microgranite, granodiorite, and feldspar-porphyritic microgranite. Although metasedimentary rocks dominate the logged sequence, the most favorable mineralized intervals are associated with felsic intrusive rocks, intrusive contacts, and quartz-carbonate veins. The principal alteration assemblage is quartz-carbonate-sericite with pyrite and arsenopyrite. Pyrite is common, but arsenopyrite is the more useful ore indicator in the available observations. Gold occurs as disseminated mineralization in intrusive rocks and locally in metasediments, and as quartz-carbonate vein-hosted mineralization.

The key petro-structural control is the interaction between the regional NNE-SSW to NE-SW Syama-Boundiali shear corridor and local NNW-SSE to N-S intrusive and vein trends. This interaction produced favorable pathways and traps for hydrothermal fluids. Further exploration should prioritize intrusive contacts, reactivated structures, and sericite-carbonate-arsenopyrite alteration zones within the broader Sissingué-Fimbiasso-Bagoé district.

Further work should focus on geochronology, whole-rock geochemistry, detailed ore microscopy, sulfide trace-element chemistry, fluid inclusions, and stable isotopes. These methods are required to test the proposed model and separate host-rock control from fluid source and mineralization timing.

Data Availability and Limitations

The Au_cat table was used only as a mineralization-class dataset. Continuous grade statistics were calculated only from selected intervals containing numerical Au values and were not extrapolated to the whole deposit. The original laboratory certificates and batch-level QA/QC files were not available for this reassessment; therefore, detection limits, insertion rates, and failed-batch decisions could not be independently audited. Public resource and reserve values cited in the text come from Perseus Mining reports and are used only to frame the district context. They were not recalculated in this study.

Acknowledgements

The authors acknowledge Perseus Mining CI for the availability of Sissingué drillcore, lithological, assay-category, structural, and section datasets used in this study. The authors also acknowledge the Laboratory of Geology, Mineral Resources and Energy, UFR Sciences de la Terre et des Ressources Minières, Université Félix Houphouët-Boigny, for the technical support provided during the petrographic and metallographic observations. Also, thank the PETROCI laboratory for support in petrographic and metallographic preparation. The constructive comments from reviewers and editors are acknowledged for improving the quality of this manuscript. AI-assisted language tools were used for editorial support only;

all analysis, interpretations and conclusions remain the responsibility of the authors.

Author Contributions

Conceptualization, O.R.M. and K.A.D.K.; methodology, O.R.M., and K.A.D.K.; data curation, O.R.M., K.A.D.K. and N.E.S.T.; petrographic and structural interpretation, O.R.M., M.E.A. and A.N.K.; writing-original draft preparation, O.R.M. and K.A.D.K.; writing-review and editing, all authors. All authors have read and agreed to the revised version of the manuscript.

Conflicts of Interest

The authors declare no conflicts of interest regarding the publication of this paper.

References

[1] Bessoles, B. (1977) Géologie de l'Afrique, Le craton ouest-Africain. Mémoires du BRGM, 402 p.

[2] Leube, A., Hirdes, W., Mauer, R. and Kesse, G.O. (1990) The Early Proterozoic Birimian Supergroup of Ghana and Some Aspects of Its Associated Gold Mineralization. *Precambrian Research*, **46**, 139-165. https://doi.org/10.1016/0301-9268(90)90070-7

[3] Milési, J.P., Ledru, P., Feybesse, J.L., Dommanget, A. and Marcoux, E. (1992) Early Proterozoic Ore Deposits and Tectonics of the Birimian Orogenic Belt, West Africa. *Precambrian Research*, **58**, 305-344. https://doi.org/10.1016/0301-9268(92)90123-6

[4] Feybesse, J.L., Billa, M., Guerrot, C., Duguey, E., Lescuyer, J.L., Milesi, J.P., *et al.* (2006) The Paleoproterozoic Ghanaian Province: Geodynamic Model and Ore Controls, Including Regional Stress Modeling. *Precambrian Research*, **149**, 149-196. https://doi.org/10.1016/j.precamres.2006.06.003

[5] Pouclet, A., Doumbia, S. and Vidal, M. (2006) Geodynamic Setting of the Birimian Volcanism in Central Ivory Coast (Western Africa) and Its Place in the Palaeoproterozoic Evolution of the Man Shield. *Bulletin de la Société Géologique de France*, **177**, 105-121. https://doi.org/10.2113/gssgfbull.177.2.105

[6] Goldfarb, R.J., Groves, D.I. and Gardoll, S. (2001) Orogenic Gold and Geologic Time: A Global Synthesis. *Ore Geology Reviews*, **18**, 1-75. https://doi.org/10.1016/s0169-1368(01)00016-6

[7] Assie, K.R., Tani, K.F., Dago, A.G.B. and N'Dri, K.A. (2024) Petro-Structural Signature and Gold Mineralization Relationship in the Meridional Sector of the Fettékro Greenstone Belt, Central-Western Côte d'Ivoire, Based on Remote Sensing and Field Investigations. *Afrique Science*, **24**, 39-56.

[8] Nestor, H.N., Koffi, A.M.P., Ephrem, A.M., Kouakou, K.K.W. and Cyrille, L.G.F. (2022) Evaluation of the Geological and Metallogenic Potential of Koffissiokaha Permit, Area of Katiola, Côte d'Ivoire. *Open Journal of Geology*, **12**, 767-786. https://doi.org/10.4236/ojg.2022.1210037

[9] Koffi, K.D., Kouassi, B.R., Koffi, G.R.S. and Allialy, M.E. (2025) Petro-Structural and Metallogenic Study of the Kimoukro and Kokumbo Geological Formations (Côte d'Ivoire, Wac). *Open Journal of Geology*, **15**, 568-585. https://doi.org/10.4236/ojg.2025.159028

[10] Pierre, K.M.J., Gbele, O. and Alexis, N.D.K. (2025) Nouvelles données pétro-structurales du sillon volcano-plutono-sédimentaire de Marabadiassa-Katiola (Centre de la Côte

d'Ivoire). *International Journal of Innovation and Applied Studies*, **46**, 1-16.

[11] Kouadio, F.J.H., Mondah, O.R., Kouamelan, A.N., Beugré, A.R., Courderc, P. and Kakou, B.F. (2026) Lithological and Structural Control of the Gold Mineralization of the Souwa Prospect (Doropo), Northeastern Côte d'Ivoire. *International Journal of Geosciences*, **17**, 478-503. https://doi.org/10.4236/ijg.2026.177023

[12] Lycopodium Minerals Pty Ltd (2015) Sissingué Gold Project, Côte d'Ivoire: National Instrument 43-101 Technical Report. Perseus Mining Limited.

[13] Perseus Mining Limited (2026) Sissingué Complex. Perseus Mining Limited. https://perseusmining.com/sissingue-complex/

[14] Perseus Mining Limited (2026) Exploration: Organic Growth Pipeline. Perseus Mining Limited. https://perseusmining.com/exploration-organic-growth-pipeline/

[15] Perseus Mining Limited (2025) Group Mineral Resources and Ore Reserves as at 30 June 2025. Perseus Mining Limited. https://perseusmining.com/resources-reserves/

[16] Perseus Mining Limited (2026) December 2025 Quarter Report. News Release. https://perseusmining.com/wp-content/uploads/2026/01/03049898.pdf

[17] Mondah, O.R. (2019) La mine de Sissingué. Éditions universitaires européennes.

[18] Graham, S. (2010) Regional Geological Compilation of the Tengrela-Sissingué Area, Northern Côte d'Ivoire.

[19] Occidental Gold SARL (2002) Tengrela Project, Property Review and Work Report. Internal Company Report, 249 p.

[20] Djagre, L., Koffi, B.G., Camara, M., Ouattara, G. and Agbossoumonde, Y. (2023) The Metasedimentary-Hosted Nyangoubé Gold Prospect, Northwest Côte d'Ivoire: Geochemical and Mineralogical Characterization of Associated Hydrothermal Alteration. *Heliyon*, **9**, e20227. https://doi.org/10.1016/j.heliyon.2023.e20227

[21] Djagre, L., Ali, K., Kra, L.K. and Koffi, B.G. (2025) Geological Controls on Gold Mineralization of the Nyangboué Prospect in the Southern Part of the Boundiali-Syama Belt, Northwest Ivory Coast. *Scientific African*, **27**, e02584. https://doi.org/10.1016/j.sciaf.2025.e02584

[22] Olson, S.F., Diakite, K., Ott, L., Guindo, A., Ford, C.R.B., Winer, N., *et al*. (1992) Regional Setting, Structure, and Descriptive Geology of the Middle Proterozoic Syama Gold Deposit, Mali, West Africa. *Economic Geology*, **87**, 310-331. https://doi.org/10.2113/gsecongeo.87.2.310

[23] Béziat, D., Dubois, M., Debat, P., Nikiéma, S., Salvi, S. and Tollon, F. (2008) Gold Metallogeny in the Birimian Craton of Burkina Faso (West Africa). *Journal of African Earth Sciences*, **50**, 215-233. https://doi.org/10.1016/j.jafrearsci.2007.09.017

[24] Smith, A.J.B., Henry, G. and Frost-Killian, S. (2016) A Review of the Birimian Supergroup- and Tarkwaian Group-Hosted Gold Deposits of Ghana. *Episodes*, **39**, 177-197. https://doi.org/10.18814/epiiugs/2016/v39i2/95775